Optoelectronic simulations for novel light management concepts in Cu(In,Ga)Se₂ solar cells

António J. N. Oliveira*[a,b], João R. S. Barbosa[a], André Violas[a], Jennifer P. Teixeira[a], Kevin Oliveira[a], Tomás Lopes[a,c,d,e], José M. V. Cunha[a, b, f], Marco A. Curado[a,g], Margarida Monteiro[a], Célia Rocha[a], Carlos Vinhais[a,h], Paulo A. Fernandes[a,f,i], Pedro M. P. Salomé[a,b]

[a]INL—International Iberian Nanotechnology Laboratory Avenida Mestre José Veiga, 4715-330 Braga, Portugal; [b]Departamento de Física, Universidade de Aveiro, Campus Universitário de Santiago, 3810-193 Aveiro, Portugal; [c]Division IMOMEC (Partner in Solliance) Imec Wetenschapspark 1, 3590 Diepenbeek, Belgium; [d]Institute for Material Research (IMO) Hasselt University (Partner in Solliance) Agoralaangebouw H, 3590 Diepenbeek, Belgium; [e]EnergyVille, Thor Park Poort Genk 8310 & 8320, 3600, Belgium; [f]i3N Departamento de Física da Universidade de Aveiro Campus Universitário de Santiago, 3810-193 Aveiro, Portugal; [g]CFisUC, Department of Physics University of Coimbra R. Larga, P-3004-516 Coimbra, Portugal; [h]Departamento de Física, Instituto Superior de Engenharia do Porto, Instituto Politécnico do Porto, Porto 4200-072, Portugal; [i]CIETI Departamento de Física Instituto Superior de Engenharia do Porto Instituto Politécnico do Porto 4200-072 Porto, Portugal

*antonio.oliveira@inl.int

ABSTRACT

One of the trends making its way through the Photovoltaics (PV) industry, is the search for new application possibilities. Cu(In,Ga)Se₂ (CIGS) thin film solar cells stand out due to their class leading power conversion efficiency of 23.35 %, flexibility, and low cost. The use of sub-µm ultrathin CIGS solar cells has been gaining prevalence, due to the reduction in material consumption and the manufacturing time. Precise CIGS finite-difference time-domain (FDTD) and 3D-drift diffusion baseline models were developed for the *Lumerical* suite and a 1D electrical model for SCAPS, allowing for an accurate description of the optoelectronic behavior and response of thin and ultrathin CIGS solar cells. As a result, it was possible to obtain accurate descriptions of the optoelectronic behavior of thin and ultrathin solar cells, and to perform an optical study and optimization of novel light management approaches, such as, random texturization, photonic nanostructures, plasmonic nanoparticles, among others. The developed light management architectures enabled to push the optical performance of an ultrathin solar cell and even surpass the performance of a thin film solar cell, enabling a short-circuit current enhancement of 6.15 mA/cm² over an ultrathin reference device, without any light management integrated.

Keywords: CIGS Technology, Light management, *Lumerical*, FDTD, SCAPS, *Lumerical CHARGE*

1. INTRODUCTION

Currently, Cu(In,Ga)Se₂ (CIGS) thin film solar cells are a mature photovoltaic technology, with a power conversion efficiency world record value of 23.35 % [1]. In the last decade, CIGS thin film solar cells world record efficiency value was surpassed 11 times, showing the technology's notable progress [2]. Nonetheless, CIGS is a complex quaternary compound, being its solar cell architecture no less complicated [3,4]. The technology evolution results from a continuous search, exploration, and implementation of different approaches to improve CIGS optoelectronic properties, such as: out of stoichiometric growth, alkali doping, bandgap engineering, among others [5,6].

The CIGS exquisite optoelectronic properties and well-established performance raised the interest in an additional branch to thin film technology, where a drastic decrease of the CIGS layer thickness from a thin (2000 nm) absorber to a sub-micrometer range, has been developed, welcoming the ultrathin technology. Regardless of the additional fundamental and technological challenges, which were brought up from a CIGS thickness lower than the necessary for a complete solar spectrum harvested in the absorber, the transfer to an ultrathin technology requires a deep knowledge on the thin film solar cell technology.

Computational simulation, or also called *in-silico* experiments, has become widely accepted as "Third Pillar of 21st Century Science", along with theory and experimentation. Within this framework, the CIGS technology has used accurate and efficient optical and electrical simulations to better understand and overcome the complexity of the CIGS solar cell system and for orientation through novel research directions [7–14]. To extend the CIGS understanding from the thin to an ultrathin thickness range, while maintaining the performance of the solar cell, optical and electrical simulations play a key role on understanding the difference in several phenomena, such as, light propagation, interface scattering, and carrier dynamics. However, an accurate output from the employed simulations is undoubtedly dependent on the need of the device modelling to keep pace with the technology evolution.

In this manuscript, a combination of optical and electrical simulations is presented, in order to describe the two main phenomena governing a solar cell's working principle: light absorption and charge carrier collection. For that purpose, and considering that we are modelling light interaction in a medium with a thickness comparable to the light wavelength values, a finite-difference time-domain (FDTD) method that solves Maxwell's equations in the time domain was performed with the *Lumerical* commercial software suite [15]. The optical properties from *Lumerical* FDTD were used to feed the one dimensional Solar Cell Capacitance Simulator (SCAPS). This robust software developed at the University of Gent, is freely available, and used to numerically simulate different types of solar cells [8,16–18]. For CIGS technology, SCAPS has been used to study the influence of physical and electronic parameters from the different layers on the output performance of the solar cell. A robust CIGS SCAPS model that describes today's technology for a thin film approach is presented. Complementing the electrical studies performed with SCAPS, simulations were conducted using *Lumerical CHARGE*, a highly versatile three-dimensional (3D) charge transport simulator. It is capable of ingesting the highly precise FDTD results and simulate accurately complex structures. Furthermore, *Lumerical CHARGE* allows for the solar cell's architecture to be optimized not only for increased optical gains, but for a superior electrical performance as well.

This manuscript presents three sections in addition to the introduction and the conclusion: FDTD Optical Simulation Model, FDTD Simulations for Solar Cell Light Management Architectures, and Electrical Simulations Support. In the FDTD Optical Simulations Section a complete overview of the optical simulations model with the demonstration of all the possible obtainable physical quantities is demonstrated. In the FDTD Simulations for Solar Cell Light Management Architectures Section, several suitable light management strategies integrated in CIGS ultrathin solar cell are reviewed and optimized in order to outperform its thin film counter-part. Finally, In the Electrical Simulations Support is shown how FDTD simulations output are of paramount importance to accurately describe electrically thin and ultrathin CIGS solar cells with conventional and non-conventional architectures using two electrical simulators, SCAPS and *Lumerical CHARGE*. This manuscript shows 3D FDTD simulations potential in the study of charge carrier generation in thin and ultrathin CIGS solar cells, as well as an exploratory tool to evaluate the impact of CIGS exotic architectures for light management incorporation. In summary, it was shown that an accurate optical description of the devices is the first step to more complex simulations to evaluate and understand solar cell principles of operation and respective performance.

2. FDTD OPTICAL SIMULATION MODEL

The optical simulations were performed by a 3D solver of the Maxwell equations, more precisely the FDTD method, which enables the resolution of the Maxwell equations in complex geometries, providing direct space and time solutions [15,19]. The FDTD solutions package available in the *Lumerical* software was used to perform the optical simulations [20]. The FDTD solutions method recurs to Fourier transforms to accurately calculate the frequency dependent electromagnetic fields, returning the complex valued fields and normalized transmissions as a function of wavelength [19]. The FDTD method is used in this work to optically describe CIGS solar cells. The typical reference solar cell architecture consists on the following structure: Mo (350 nm), MoSe$_2$ (5 nm), CIGS, CdS (50 nm), i-ZnO (100 nm) and Al:ZnO (AZO) (400 nm). In Figure 1 a schematic representation the described CIGS solar cell stack with a typical thin (2000 nm) and ultrathin (500 nm) absorber is shown in a) and b), respectively. In this Section, the potential of the optical model used is explored through the demonstration of all the physical parameter values possible to be extracted by the simulation model.

In order to simulate the solar cell stack, the complex refractive index ($n(\lambda) = n + ik$), the refractive index n and the extinction coefficient k, of each material needs to be used as input. The CIGS, with [Ga]/[Ga+In] (GGI) = 0.3, optical properties were obtained through in-house spectroscopic ellipsometry measurements. The AZO, i-ZnO, and CdS compounds were taken from reference [21], the MoSe$_2$ layer from [22], and the Mo layer from [23]. A broadband plane wave source is used to introduce a uniform electromagnetic field into the solar cell stack in a wavelength range from 300 to 1100 nm. Depending on the simulated solar cell architecture, different Cartesian mesh sizes have been used. However, the mesh size considered is the smallest possible to respect the memory and time requirements of each simulation. Furthermore,

override mesh regions are commonly used at critical interfaces or nanostructures to provide the best simulation accuracy. Typically, the simulated structures present periodicity, and, therefore, to reduce the simulation time, symmetric and anti-symmetric boundary conditions are also used, enabling to simulate only ¼ of the total space.

The FDTD optical simulation software allows for the calculation of the total light absorbed in each layer. For that purpose, the power absorbed per unit volume (P) is calculated in each layer, as following [24]:

$$P = \frac{1}{2}\omega\varepsilon''|E(\lambda)|^2 \tag{1}$$

where, ω is the angular frequency, ε'' the imaginary part of the dielectric permittivity, and $|E(\lambda)|^2$ is the electric field intensity as a function of the wavelength value. The light absorbed in each layer per wavelength value ($Abs(\lambda)$), is then calculated through the integration of the normalized P over the solar cell spectrum. Using $Abs(\lambda)$, a spectrum containing the absorption in each layer of the solar cell stack is obtained, as demonstrated in Figure 1 a) and b) for thin and ultrathin CIGS solar cells, respectively. These plots are essential to accurately evaluate the solar cell optical performance, as it enables the verification of individual layers' optical losses at specific wavelength values, as well as, to check improved optical performances, obtained through the integration of light management structures. For the studied CIGS architectures, the light collection by the absorber layer is significantly reduced due to parasitic absorption in the solar cell remaining layers. The transparent conductive oxides (TCO), both in the thin and ultrathin configuration, demonstrate a significant parasitic absorption in both UV and NIR regions. Through the optimization of the contact layer thicknesses, this parasitic absorption can be reduced [25]. The CdS parasitic absorption stems from the relatively low bandgap energy value of this buffer layer (~2.4 eV) [26], and is as well thickness dependent. Other buffer materials that have larger bandgap energy values are currently being investigated in CIGS solar cell devices [27,28]. Notably, the solar cell architecture that led to the CIGS solar cell world record efficiency value (23.35 %) uses an $Zn(O,S,OH)_x$ /$Zn_{0.8}$ $Mg_{0.2}$ buffer layer [1]. An increase in the detrimental absorption in the Mo layer, as the absorber thickness is reduced from 2000 to 500 nm is observed. Such parasitic absorption is an indication that ultrathin CIGS absorbers are unable to fully absorb the incoming light in one single passage. Thus, light management architectures need to be developed to increase the optical path inside the CIGS absorber, as will be shown in Section 2.
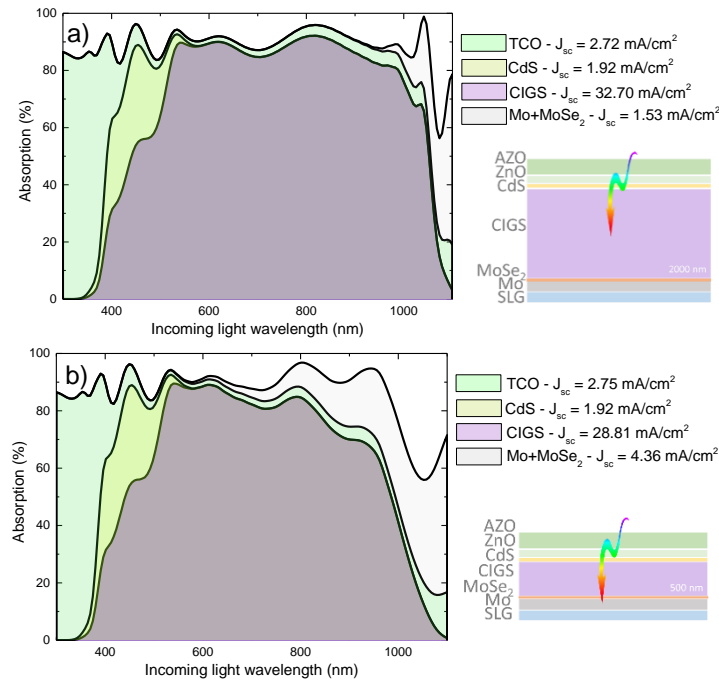

Figure 1. Absorption in the solar stack layers and schematic CIGS solar stack representation for a) thin (2000 nm) and b) ultrathin (500 nm) absorber.

From the absorbed light, quantities like the charge carrier generation rate (G) and short-circuit current density (J_{sc}) can be obtained, through

$$G = \int_{\lambda_{min}}^{\lambda_{max}} \frac{\lambda}{hc} \text{Abs}(\lambda)\, I_{AM1.5G}(\lambda) d\lambda \qquad (2)$$

$$J_{sc} = qG \qquad (3)$$

where, h is the Planck's constant, c is the speed of light, $I_{AM1.5G}(\lambda)$ is the AM1.5G solar spectrum and q is the elementary charge. A quantification of the solar cell's optical performance is defined by its J_{sc} value. This value will be the maximum current density that the CIGS solar cell will achieve considering only the optical properties of the solar cell architecture, disregarding non ideal effects on the transport and extraction of charge carriers. The G parameter may be represented in 1D or 2D profiles as a function of position and/or incoming light wavelength values, as represented in Figures 2 for CIGS thin a) / c), and ultrathin b) / d), respectively.
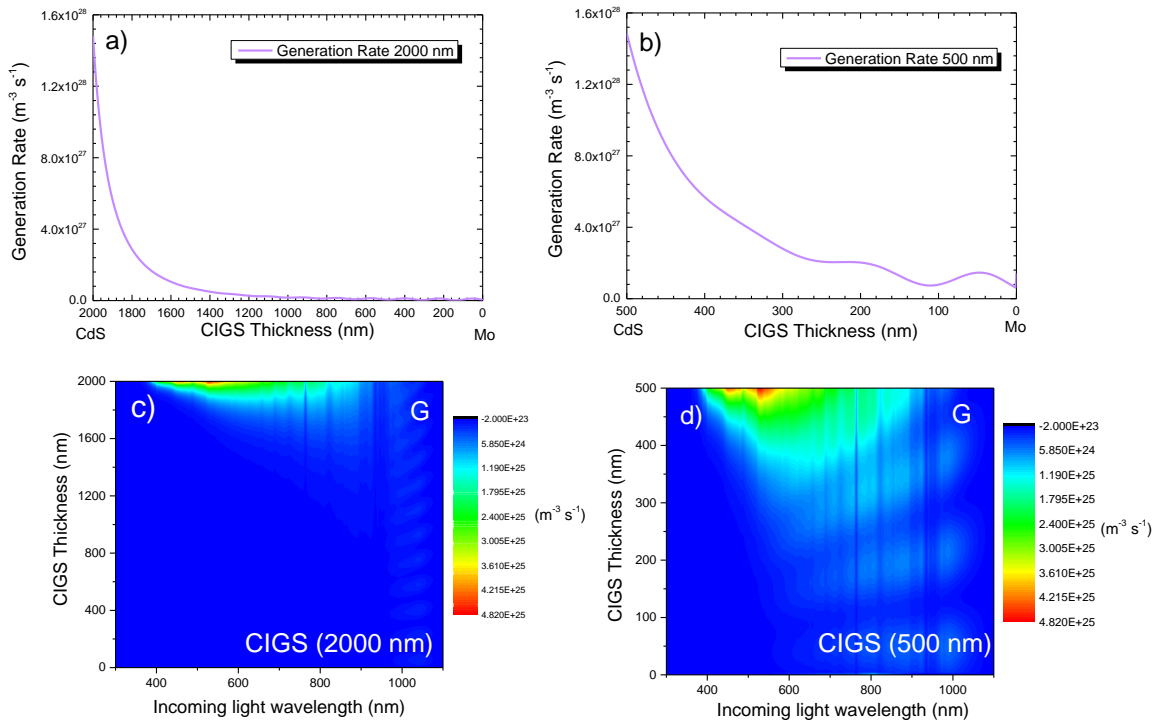

Figure 2. 1D Generation rate profile as a function of CIGS thickness in, a) a thin (2000 nm) and b) ultrathin (500 nm) absorber; 2D Generation rate profile as a function of the incoming light wavelength in: c) a thin and d) ultrathin absorber.

A transmission monitor is always placed above the solar cell stack, to quantify the total solar cell reflection (Figure 3 a)), which can be used to evaluate anti-reflection properties as well as light trapping effects of different light management architectures. In this case, in the ultrathin absorber (500 nm) there is a higher reflectance at the NIR wavelength range, stemming from light leaving the solar cell after being reflected from the back contact, that otherwise would be absorbed in the thicker 2000 nm absorber. The electric field intensity profile in the absorber layer (Figure 3 b)) or at any other layer/interface, giving insight into the effect of light concentration or scattering by different nanostructures used for light management, can also be obtained. A Transfer Matrix analytical formalism is used to validate the reference solar stack simulations accuracy, through the comparison of the simulated light absorption in the solar cell stack with the calculated absorption from the Transfer Matrix Analytical formalism (Figure 3 c)). The almost perfect overlap between the simulated and analytical absorptions, demonstrate the accuracy and viability of these simulations and opens the door for more complex geometries and exotic light management architectures. The optical performance of a solar cell stack with complex geometries can be fully characterized through all the simulated quantities presented in this Section. Furthermore, various

parameters obtained from the optical simulations can be used to improve the accuracy of electric simulations performed either with SCAPS or *Lumerical* CHARGE, as it will be shown in Section 3.
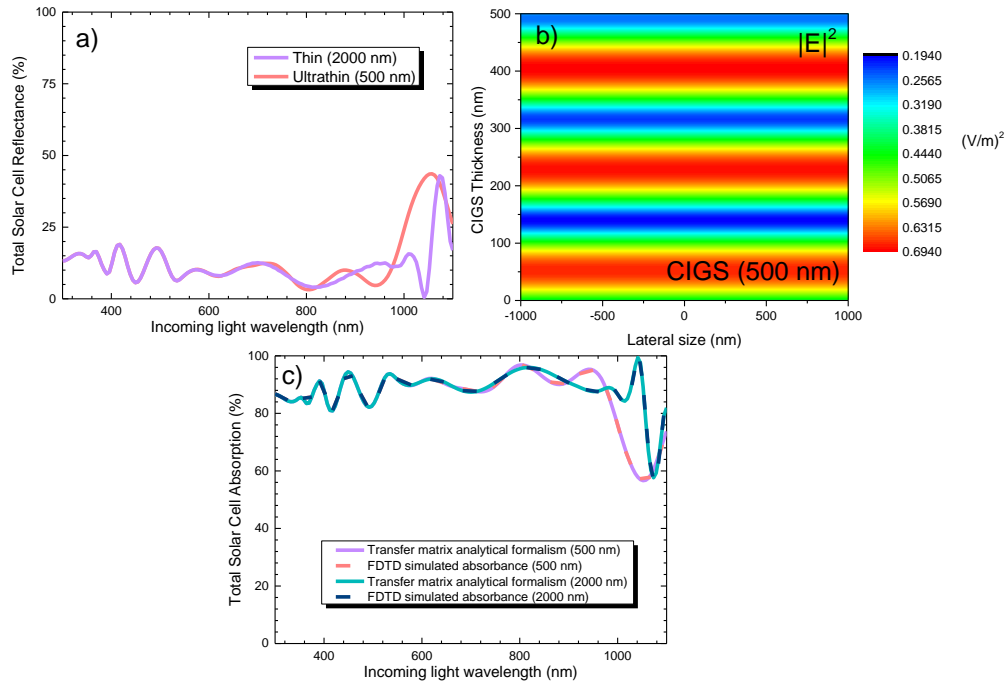

Figure 3.a) Total solar cell reflection of both the thin and ultrathin devices; b) Electric field intensity profile in an ultrathin absorber at a specific y plane in the CIGS absorber; and c) Total solar cell absorption from the transfer matrix formalism and from the FDTD simulation in an thin and ultrathin solar cell devices.

3. FDTD SIMULATIONS FOR SOLAR CELL LIGHT MANAGEMENT ARCHITECTURES

One of the biggest challenges to attain conversion efficiency values that match the Shockley-Queisser limit is the optical losses present in solar cell devices [29]. Light reflection, parasitic absorption and absorption losses that either prevent the entrance of light in the absorber material or hinder an efficient light absorption, need to be minimized [25]. Light trapping schemes are then essential to enhance the efficiency of solar cell devices. Their integration may be done through many ways, with the intent of increasing the solar cells efficiency value, by reducing the external reflection of light and increasing the internal optical path length. Over the past years, light trapping architectures have been thoroughly studied for application in thin film solar cells, since it allows them to be viable competitors to their bulk counter-parts [30–32]. Applying light trapping structures in a solar cell allows for the absorption of the same quantity of sunlight in a much thinner absorber material, which leads to a reduction of material and production costs on photovoltaics (PV) devices, helping the mass production of solar cells composed by scarce materials, such as, CIGS and CdTe solar cells [33]. In this Section, a review on light management schemes that can be exploited to boost the optical performance of an ultrathin CIGS solar cell stack is performed, recurring to highly precise 3D optical FDTD simulations. Currently, thin film CIGS solar cell modules have an absorber thickness of about 2000 nm. Economical and sustainable industry imposed goals drive the reduction of the absorber thickness to sub-micrometre thicknesses, in what is called the ultrathin regime [33]. In Figure 4, the light absorbed in two typical CIGS solar cell stacks (reference), with an absorber thickness of 2000 nm (thin) and 500 nm (ultrathin) without any light management architectures is shown. At longer wavelengths (600 to 1100 nm), the optical performance of the thinner absorber starts to degrade in comparison to the 2000 nm thick absorber. Such effect is related to the incomplete light absorption by the solar cell absorber, as the CIGS layer is not sufficiently thick to accommodate the penetration depth of NIR light in one single pass. By reducing the absorber thickness from 2000 nm down to 500 nm an almost 4 mA/cm^2 loss on the J_{SC} value is observed. In order to achieve or surpass the optical performance of conventional 2000 nm CIGS solar cell stacks two main issues may be tackled: (1) reflection at the front surface and (2) poor absorption at the NIR range.
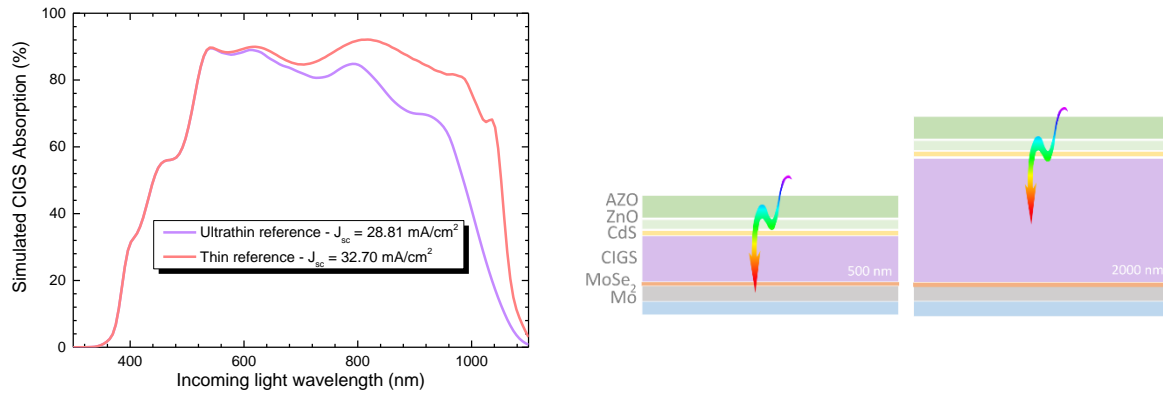
Figure 4. Simulated CIGS absorption of two solar cell stacks with 2000 and 500 nm absorber layer thickness and the obtained J_{SC} value of 32.70 and 28.81 mA/cm^2, respectively. Schematic representation of the CIGS solar cells stack architectures.

Despite of the typical CIGS architecture having an AZO/i-ZnO/CdS top layer stack, that already offers a good n match with the absorber, various strategies can be implemented to achieve a better anti-reflection performance [25]. The most simple and common approach consists of using interference type Anti-Reflection (AR) layers at the top of the solar cell device [34,35]. These thin dielectric layers can successfully minimize reflections at specific wavelength values by allowing a destructive interference of the light reflected from the front and rear sides of the AR layer [35]. In order to do so, the thickness of the AR layer (d_{AR}) should correspond to one quarter of the wavelength range to be minimized:

$$d_{AR} = \frac{\lambda_0}{4n_1} \tag{4}$$

where λ_0 is the wavelength value for optimization and n_1 is the AR layer refractive index. Normally an MgF$_2$ anti-reflection layer ($n = 1.4$ at 600 nm) is used in laboratory CIGS solar cells, as it allows for a good refractive index match between the air ($n = 1$) and the AZO contact ($n = 1.9$ at 600 nm). To optimize the performance of an MgF$_2$ AR layer, a particle swarm optimization algorithm included in the FDTD solutions software was used [35]. With this approach, the AR layer thickness was optimized to attain the maximum J_{SC} value in a CIGS ultrathin solar cell. In Figure 5, simulated CIGS absorption in an ultrathin device with and without the optimized MgF$_2$ reflection layer is shown, alongside the simulated reflectance. The optimized MgF$_2$ thickness corresponds to 114 nm. With the implementation of a 114 nm MgF$_2$ layer, an overall broadband anti-reflection improvement is achieved, as shown by the reduced reflection throughout the simulated spectrum in Figure 5, leading to a J_{SC} improvement of 2.59 mA/cm^2.
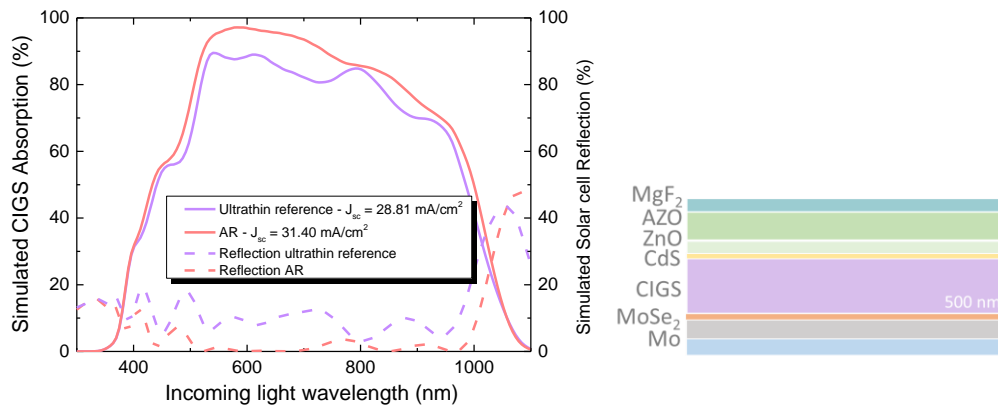

Figure 5. Simulated CIGS absorption and total solar cell reflection of an ultrathin reference and ultrathin solar cell with an optimized AR layer. Schematic representation of the CIGS solar cells stack architecture with an MgF$_2$ AR layer implemented.

Another anti-reflection approach consists in introducing texturization on the solar cell top layers. To study the optical benefits of such approach, two different architectures were implemented and studied by FDTD simulations: i) one consisting on a random texturized AZO surface, that can practically be achieved in wet-etching procedures through acidic solutions, enabling an anisotropic etching [36–39]; ii) an approach with higher fabrication complexity, consisting on a nanostructured AZO layer with a periodic 2D triangular grating.

The random texturization was implemented by using the surface roughness structure present in the FDTD *Lumerical* software object library. This object allows to modulate the surface roughness through the control of two parameters, the specified RMS roughness (σ_{RMS}) and correlation length (L_c), which determines the overall size of the craters at the surface - a surface with a large L_C value will be smother and with larger craters, than a surface with a small L_c value. In initial studies, it was verified that the AR performance is enhanced both by increasing the σ_{RMS} and decreasing the L_c values, therefore the optimization goes on establishing a lower surface roughness limit. For these simulations, a σ_{RMS} value of 100 nm and a L_c of 100 nm, that is in accordance with the structural features verified in wet-etch procedures of ZnO and AZO layers in acidic solutions, was applied to the 400 nm AZO layer [40–42]. The simulated absorption in the CIGS layer, alongside the simulated reflection, for an ultrathin reference and an ultrathin device with a random textured AZO layer device are shown in Figure 6 a). With random texturization, a J_{SC} value of 32.09 mA/cm^2, which corresponds to a 3.28 mA/cm^2 increase over the ultrathin reference device, was obtained. The J_{SC} enhancement is due to the improvement of the AR behavior with an increasingly rougher surface, as seen by the broadband decrease of the measured reflectance. This is shown in Figures 6 b) and c), where the electric field intensity at the top surface of the ultrathin reference solar cell and the random texturized surface at 600 nm, respectively, is shown. In Figure 6 b) interference fringes stemming from the interaction between the incident light with the light reflected from a perfectly flat surface are present, while in Figure 6 c) the reflection is significantly decreased with the textured surface. Thus, having a rougher surface gives rise to an increased number of multiple reflections in the created slopes leading to the improvement of the AR properties of the solar cell.
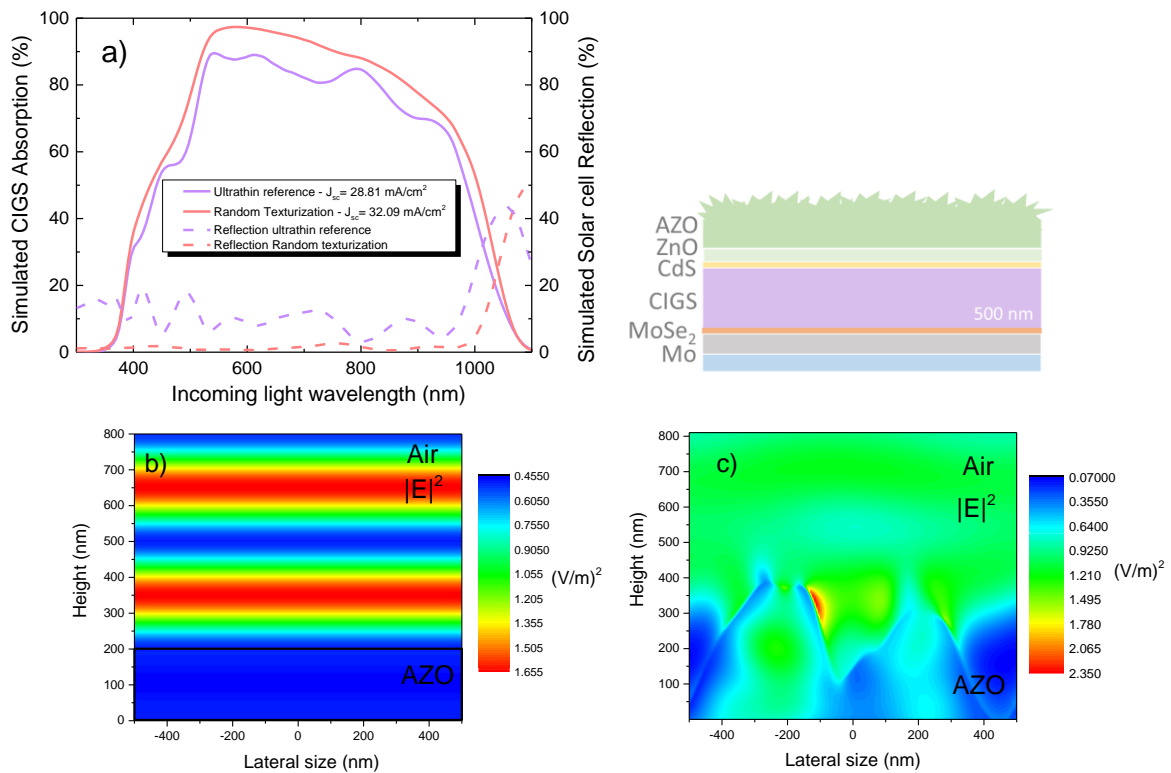
Figure 6. a) Simulated CIGS absorption and total solar cell reflection of an ultrathin reference and ultrathin solar cell with an optimized random texturized AZO layer; and electric field intensity at 600 nm on the air/AZO interface for b) an ultrathin reference and c) an ultrathin solar cell with an optimized random texturized AZO layer. Schematic representation of the CIGS solar cell stack architecture with a random texturized AZO layer.

An alternative approach is the use of nanoscale periodic structures. With such periodic structures, a more precise control over the light management mechanisms can be achieved, just through the variation of some morphological parameters [43]. When the texture periodicity (Λ) is much larger than the incident wavelength ($\Lambda \gg \lambda$), the light will be scattered into various diffraction orders [44]. The intensity of such diffraction orders depends on the texture's shape and height. This contributes to an enhancement of the optical path length at the absorber layer, as the light enters the solar cell in oblique directions [44]. However, such scattering effects also enable a larger optical path in the solar cell window and buffer layers, increasing the parasitic absorption in these layers [45,46]. Furthermore, such large periodic structures enable multiple reflections within the large textures allowing for a reflection decrease [44]. When the structural features present critical dimensions much smaller than the incident wavelength ($\Lambda \ll \lambda$), the light is not scattered into different diffraction orders, but rather achieves the best anti-reflection performance. This happens because with such small dimensions, the effective medium theory predicts that the nanostructures behave as a single layer with a refractive index optimized to achieve a broadband AR behavior [44]. In order to demonstrate this light management concept, optical simulations of a solar cell stack with a 2D triangular trench pattern on the AZO were performed. For this approach, different period values were used in the trench pattern with a height of 300 nm, to demonstrate effect of this morphological parameter on light guidance. The first approach was to simulate different period values to demonstrate the two extreme cases ($\Lambda \gg \lambda$ and $\Lambda \ll \lambda$). For this purpose, a period of 50 and 1000 nm were chosen. For the latter value, the simulation memory and time requirements were considered, as increasing the period involved a larger simulation volume that would be unfeasible. In Figure 7 a) and b), the electric field intensity inside the absorber layer is represented at a wavelength value of 1000 nm, for both the 50 and 1000 nm period. Both representations demonstrate interference effects, that happen because the simulated absorber only has 500 nm, so inevitably, a portion of the light will be reflected from the Mo rear contact back to the absorber creating the observed interference fringes. The most important observation from the electric field profiles, is that the 50 nm period structures behave collectively as a flat surface, as predicted by the effective medium theory [44], while in the structure with a period of 1000 nm a clear diffraction effect from the triangular grating can be verified. The absorption and reflection of both structures were simulated and compared with the ultrathin reference device, as shown on Figure 7 c). From the simulated reflection values, it is clear the better AR response arising from the nanoscale texturization, as a reflection close to 0 % is achieved for the majority of the region of interest of the solar spectrum. As explained before, this broadband AR effect arises from the small dimensions of the nanoscale texturization in comparison with the wavelength value. The nanoscale features behave as if light interacts with a homogeneous medium with a gradual refractive index, more precisely as if multiple thin ARC layers are stacked on top of each other with an optimal refractive index profile [47]. The reflection increase over the NIR wavelength range can be justified from the light reflected in the back contact and exits the solar cell through the top surface. The slight absorption increases in the NIR region, as well as the lower reflection values at this range, demonstrate the better scattering performance of the texturized structure with 1000 nm period. The better AR performance of the solar cell device with a 50 nm period led to a 3.6 mA/cm^2 increase of the J_{SC} value, over the ultrathin reference solar cell. However, the complexity of a periodic structure with 50 nm period may hinder the fabrication of such texturized surface, as it is hard to achieve this dense array of nanostructures with a high aspect ratio over large areas.
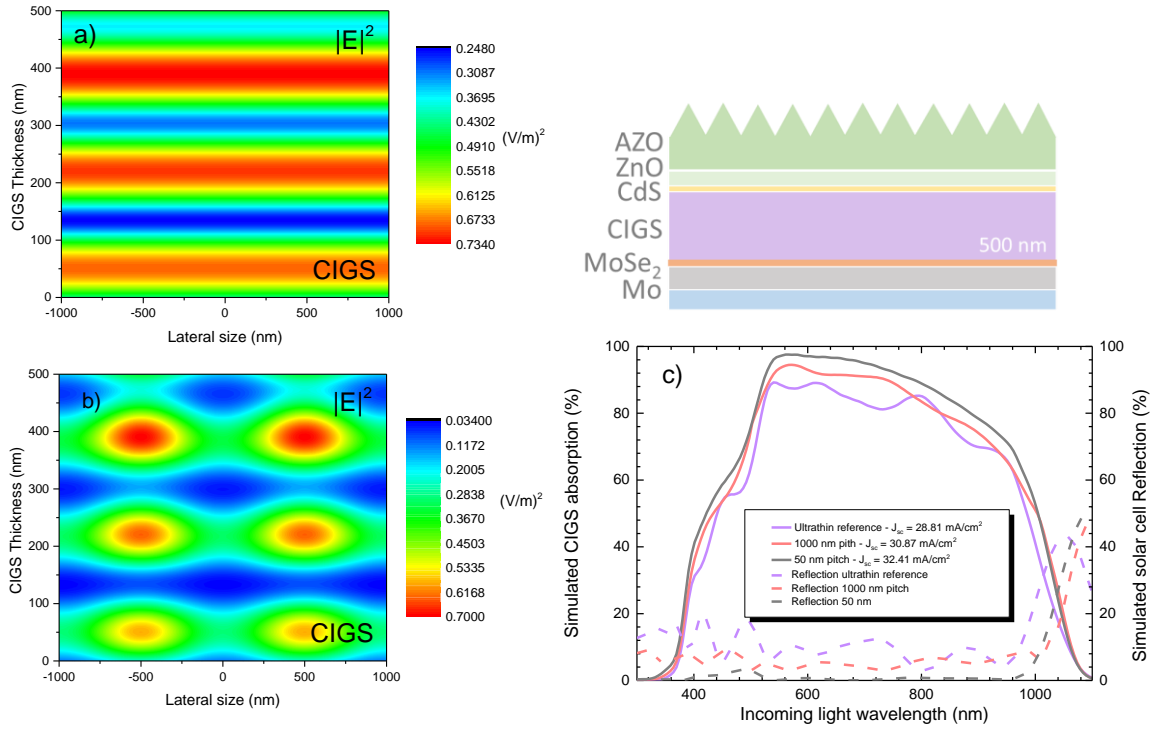
Figure 7. Electric field intensity at 1000 nm in the CIGS layer for a) periodic structure with a 50 nm period and b) periodic structure with a 1000 nm period; c) simulated absorption in the CIGS layer and total solar cell reflection in the three different studied architectures: 2D triangular grating with a 50 nm period, 2D triangular grating with a 1000 nm period and a reference solar cell with no texturization. Schematic representation of the CIGS solar cells stack architecture with a 2D triangular array pattern AZO layer.

Another critical optical loss is the poor light absorption in the NIR region. To tackle such issue, light management strategies are employed to enhance the optical path length inside the absorber layer. Light management architectures can be employed at the back interface and enhance this interface reflection/scattering capabilities. The simpler approach consists of adding a highly reflective metallic layer as the solar cell back contact, enabling to double the light optical path inside the solar cell [25]. However, in CIGS solar cell devices, employing highly reflective layers, such as Al, Ag or Au can be difficult. During the absorber deposition, the metals are submitted to high temperatures and may diffuse to the absorber layer, or react with Se, degrading the solar cell electrical performance [14,48]. Commonly a Mo layer is used as back contact, which is a more chemically and thermally stable metal. Nevertheless, the Mo reflection lacks in comparison with other metals, such as the one aforementioned [49–52]. To study the optical benefits of a metallic layer on a CIGS ultrathin solar cell device it is imperative that a dielectric layer is added on top of the optical mirror. The following rear contact architecture was employed: Mo/Ag (25 nm)/SiO$_2$ (20 nm). It is important to note that in this approach, the influence of a contact architecture is not studied, as a purely optical study is being performed in this Section. Furthermore, here the metal of choice is Ag, since this structure will be integrated in an architecture with Ag plasmonic nanoparticles (NPs) further down in this section. In Figure 8, the simulated CIGS absorption, alongside the total solar cell reflectance of the solar cell with the metallic layer and the ultrathin reference is presented. With the introduction of the metallic layer, there is a 1.49 mA/cm^2 improvement over the reference J_{SC} value since it allows an additional pass of the light that wasn't absorbed in the CIGS layer during the first pass. Furthermore, there is more light leaving the solar cell, as shown by the increased reflection in the NIR. However, adding the metallic layer only doubles the optical path, as it works as an optical mirror, only allowing an increase in the light's specular reflection [53,54].
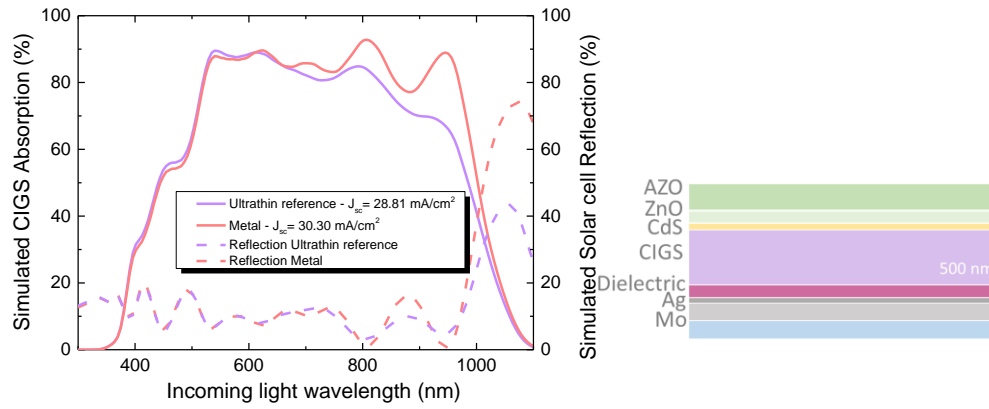
Figure 8. Simulated absorption in the CIGS layer and total solar cell reflection of the ultrathin reference and the solar cell device with the metallic layer at the rear contact. Schematic representation of the CIGS solar cells stack architecture with an Ag metallic/dielectric based substrate.

Other light trapping concepts need to be explored to further enhance the light path inside the absorber [25]. The surface texture of the back contact is also a potential strategy to increase light absorption in thin film solar cells. For example, Huang *et al.* produced in [55] a highly scattering rear Si surface texture by plasma etching of poly-Si thin film solar cells. Using the plasma-etching technique, sub-micron textures at the rear surface were produced and values of haze reflection higher than 95 % at the Si-air interface were achieved [55]. However, in thin film solar cells such texturization can degrade the overall cell performance by creating defects in the absorber material [56]. Another approach consists in exploring the plasmonic resonances of metallic nanoparticles. When light reaches the metallic nanoparticle, the electric field will lead the metal's free electrons to the nanoparticle surface. Since these entities are confined, positive charges will be accumulated at the opposite surface creating an electric dipole. This charge displacement generates an electric field that induces an oscillatory behavior of the electron cloud [57]. At certain wavelength values, the incident light can be in resonance with the metals free electrons oscillations, leading to resonant oscillations of the electron cloud that can generate high scattering or absorption cross-sections, depending on the NPs size, shape and dielectric medium [57,58]. The nanoparticle resonance can be tuned to enhance the scattering effect at the NIR region, where the thin film solar cells absorber thickness is not sufficient to accommodate the long wavelength's penetration depth. To redshift the nanoparticle resonant wavelength value, large sizes (around 50 nm radius) and elongated shapes are preferred [57,58]. Usually these plasmonic entities are integrated in the solar cell structure accompanied by a metallic layer, creating a so-called plasmonic back contact [59]. This way, the light scattered backwards by the NPs can be reemitted to the solar cell's absorber.

For a viable integration of the Ag plasmonic nanomaterials, one must study the scattering cross-sections at the localized surface plasmon resonance (LSPR). In order to do so, a total-field scattered-field (TFSF) source with a wavelength range between 300 to 1100 nm was used to illuminate Ag NPs with a radius of 50 nm. The TFSF source allows to study the scattering and absorption behavior of the spherical NPs, as it can separate the NP scattered field from the incident electromagnetic field [19]. The scattering and absorption efficiency of a NP can be calculated by normalizing the scattering (C_S) and absorption cross-section (C_A) to the NP volume, using the following equation:

$$C_{A,S} = \frac{P_{A,S}}{I_{AM1.5}} \tag{5}$$

where $P_{A,S}$ is the net power absorbed/scattered by the NP. It is important to keep in mind that the refractive index of the medium where the Ag NPs will be inserted is different than 1 (air). The CIGS absorber has a higher refractive index close to 3. Furthermore, the NPs will be encapsulated by a dielectric material. Therefore, for a proper study of the effective scattering behavior of the Ag NP (Figure 9) located inside the solar cell architecture, a refractive index of 3 was used and an oxide shell of different dielectric materials (SiO_2, Al_2O_3, and TiO_2) was placed surrounding the NP. The resonant wavelengths of the stand-alone Ag NP are within the desired NIR wavelength range. However, one must consider that the NPs cannot be implemented directly in contact with the CIGS layer, since Ag would not withstand the harsh growth conditions of the absorber. Therefore, the NPs need to be encapsulated with a dielectric layer. On the other hand, this will affect the resonant properties of this nanostructures, as the local refractive index of the medium is different. The oxide shells have a lower refractive index than the CIGS, so a blue-shift and dampening of the scattering cross-section is verified

with the implementation of every oxide shell [60]. SiO$_2$ has the lowest refractive index, leading to the largest blue-shift and dampening effect, while the opposed is verified in TiO$_2$ that has the lowest dampening and blue-shift. As such, for an improved optical performance, a TiO$_2$ shell holds more promise, as it is the configuration with the highest scattering efficiency matching the wavelength range where most optical losses will occur due to incomplete light absorption in an ultrathin solar cell device.
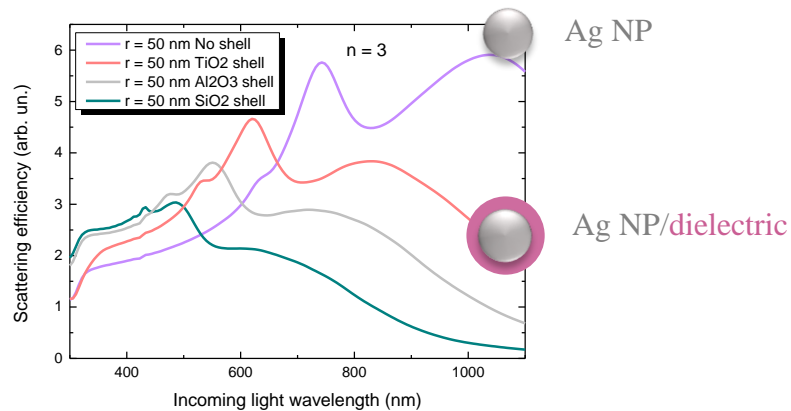

Figure 9. Scattering efficiency of 50 nm radius Ag NPs incorporated in a medium with $n = 3$: without an oxide shell, with a 10 nm SiO$_2$, Al$_2$O$_3$ and TiO$_2$ shell.

A periodic structure of Ag NPs displayed in a rectangular lattice was integrated in an ultrathin CIGS solar cell. A metallic layer was placed below the NPs, to collect the light that is scattered backwards and would be absorbed by the Mo layer. The NPs were integrated into the solar cell through a volume compensation approach, i.e. the occupied volume by the NPs was added to the thickness of the CIGS layer without any texturization transfer. This method was used to decouple the AR effects that would occur from the front-surface, if the NPs texturization was translated to the upper-most layers. Previous to the solar cell stack simulation, an optimization sweep was performed to study the best distance between the metallic NPs, in order to obtain the NP surface coverage presenting the highest scattering efficiency [61]. This optimization was achieved once again through a particle swarm optimization algorithm included in the FDTD solutions software [19]. The CIGS simulated absorption, of three solar cell devices with this plasmonic configuration is represented in Figure 10 a). When comparing the performance of the different dielectric layers, the configuration with the TiO$_2$ shell, with the highest dielectric constant, presents the highest simulated J_{SC} value (31.04 mA/cm^2). As demonstrated before, in Figure 9 when the NPs are encapsulated in a TiO$_2$ shell, the best resonant matching and the best scattering performance for a single NP is achieved. However, it is important to consider the effect of this dielectric layer in the solar cell electrical performance. While Al$_2$O$_3$ and SiO$_2$ dielectric layers have been successfully employed and extensively studied in CIGS solar cells as surface passivation layers [48,54,62–66], TiO$_2$ was not. The employment of TiO$_2$ in this optical study served, however, to demonstrate the benefits of using oxide layers with a higher refractive index. In Figure 10 b), the CIGS simulated absorption of the ultrathin reference, a solar cell stack with a metallic layer and the best performing plasmonic configuration are presented. With the plasmonic configuration, a 2.23 mA/cm^2 increase of the J_{SC} value can be achieved over a reference solar cell, and around 0.74 mA/cm^2 when compared with a structure with only a metallic layer. Such enhanced optical performance is a result of the increased scattering at the NIR wavelength range. Comparing the absorption spectrum of the solar cell with the metallic layer and the plasmonic solar cell, there is an absorption dip over the 900 nm wavelength region in the solar cell with nanoparticles. This effect is related to a fundamental limit of the plasmonic approach, since at the resonant wavelength values, the Ag NPs also present a strong absorption cross-section, leading to parasitic absorption that it is not used to generate photocurrent [25,56]. This effect is demonstrated on the higher Ag parasitic absorption in the plasmonic configuration as opposed to the metal one, also presented in Figure 10 b). Furthermore, the integration of metallic NPs can also be complex in substrate architectures, as the metal may diffuse into the absorber during its high temperature deposition [25,56]. Therefore, chemically stable and absorption-free dielectric NPs have also been a topic of interest for scattering entities in solar cell devices at the rear interface [67,68]. Besides an optical benefit, such dielectric nanostructures may provide a passivation effect beneficial for the solar cell optoelectronic properties [25].
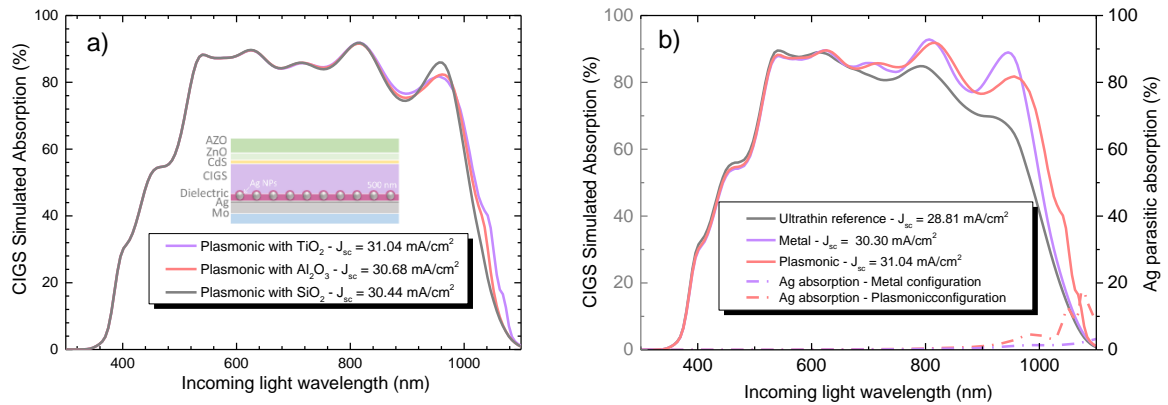
Figure 10. a) Simulated absorption in the CIGS layer on solar cell stacks with the plasmonic architecture using three different oxide layers (SiO$_2$, Al$_2$O$_3$ and TiO$_2$); b) Simulated absorption in the CIGS layer and Ag parasitic absorption in the three different studied architectures: configuration with only a metallic layer, plasmonic configuration and a reference solar cell with no light trapping architecture. Schematic representation of the CIGS solar cells stack architecture with an Ag metallic/dielectric/Ag NPs/ dielectric based substrate.

The most effective light management approaches both to reduce the front surface reflection and to increase the optical path length value were incorporated in a solar cell stack. In Figure 11 a), the simulated absorption in the CIGS layer of the optimized architecture (best texturization plus plasmonic) is compared with the reference solar cell devices (ultrathin and thin). The broadband AR performance, as well as the increased optical path length, led to a J_{sc} value of 34.96 mA/cm^2, 2.26 mA/cm^2 higher than the thin reference with 2000 nm thick CIGS. The optical path length through the employment of the best light management architectures is compared with the one of the ultrathin reference (Figure 11 b)). To calculate the optical path length, a method developed by Hegedus and Shafarmann was followed [69]. With the implementation of the plasmonic back reflector as well as from the texturized AZO layer an optical path length as high as 4 is achieved in the NIR region. The increase of the optical path length over the ultrathin reference leads to an optical absorption performance equivalent to the one verified in the NIR range in the thick 2000 nm absorber, as it is seen in Figure 11 a). Therefore, such light management architectures enable a reduction of the solar cell production costs, since a 4 times lower absorber thickness may be used without significant optical losses. Furthermore, the developed nanostructures can be produced by low-cost, industrially friendly approaches, as the trench design can be implemented through nano-imprint lithography and solution-based depositions can be used to deposit the metallic plasmonic nanoparticles.
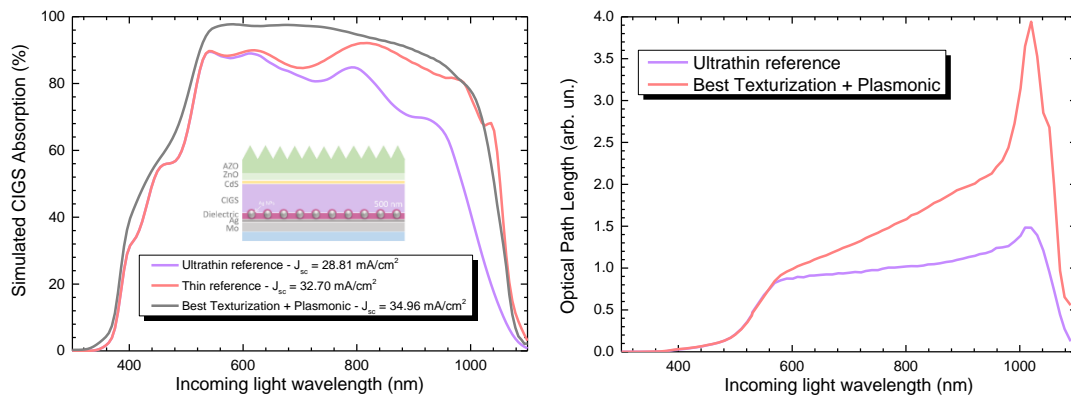
Figure 11. a) Simulated absorption in the CIGS layer on reference solar stacks with 500 and 2000 nm absorbers and in a solar cell stack where the best light management approaches were integrated b) Estimated optical path length in a solar cell stack with the best light management approaches and a reference solar cell with an absorber thickness of 500 nm. Schematic representation of the CIGS solar cells stack architecture with full optimized light management integration.

4. ELECTRICAL SIMULATION SUPPORT

The optical parameters, extracted from the analysis of a solar cell stack with the FDTD software, can be integrated into electrical simulations to obtain a fully viable optoelectronic model. In this Section, two different examples where FDTD was used to enhance electrical simulations, will be described. First, the validation of the SCAPS electrical model was performed through the comparison of the figures of merit of a simulated 2000 nm CIGS solar cell with the current conversion efficiency record holder with equivalent architecture [70]. Second, the FDTD method was used to improve the electrical simulations of a more complex solar cell architecture in the *Lumerical* CHARGE software. Here, an optoelectronic model was developed to study an ultrathin architecture with a patterned metallic/dielectric interlayer integrated at the Mo rear contact.

At first, the use of two electrical simulators, SCAPS and *Lumerical CHARGE*, to study CIGS solar cells might seem as a waste of resources. However, even though each program has its own strong points, both exhibit certain weaknesses that end up being complemented by the other software solution.

SCAPS software is a 1D solar cell and capacitor simulator, tailored for the simulation of thin film solar cells [18]. Therefore, it incorporates in its models various phenomena typically found in thin film solar cells, such as various recombination mechanisms located throughout the cell, a multitude of defects levels, and many other parameters [71,72]. The end result is the possibility to develop electrical numerical models with a high degree of correlation with real samples, which in turn, can be used to better understand the behavior of said samples, and thus, provide a pathway for improvement. Moreover, not only is this tool freely available to the PV scientific community, as it only requires modest computational resources. The consequence of these advantages is a multitude of available literature that can act as a reference and as a springboard, for one's work into highly advanced electrical studies of thin film solar cell's architectures. Nonetheless, even though SCAPS is a powerful tool, it has its own shortcomings as well. The most significant one is the fact that it can only simulate 1D architectures. If the object of study is a line contact or a point contact passivation layer for example, 2D and 3D structures respectively, SCAPS cannot accurately model said structures, requiring thus, a considerable amount of assumptions and approximations during the creation of the electrical model of the design in study. Another aspect that can be lacking, is the optical aspect of the solar cell simulations, as it only accounts for simpler optical models and phenomena when compared with more specialized optical simulation software, whereas the outsourcing of reliable optical data is necessary for such SCAPS models.

The *Lumerical CHARGE* electrical simulator is built on the finite element drift-diffusion method and it is capable of performing 2D and 3D simulations of custom and highly complex structures. In the case of solar cells, it takes into consideration the complex optical response of the entire solar cell architecture, by importing the charge carrier generation rate distribution calculated with *Lumerical* FDTD. The end result is that *CHARGE* cannot only calculate the conventional figures of merit, but it also provides a multi-dimensional distribution of the variation of multiple parameters throughout the solar cell, such as the band structure, carrier current density, free charge density, electric fields, recombination, carrier's lifetime and so on. The ability to incorporate the results of complex thermal simulations, performed with *Lumerical HEAT* is available as well, thus allowing the study of the impact of the thermal response of a solar cell in its own behavior. Additionally, the *Lumerical* simulation suite offers the possibility to use Particle Swarm optimization algorithms, or other custom algorithms, to better exploit the available computational resources, and aid the architectural design. However, once again, this software tool has its own constraints. Unlike SCAPS, *Lumerical CHARGE* requires the purchase of software licenses, thus restricting those who can access it. Furthermore, the ability to perform multidimensional simulations comes at a cost of high computational requirements. As a consequence, this tool is only infrequently found in the thin film PV literature. Since *Lumerical CHARGE* was designed with a more universal application range in scope, even though this approach has several advantages, it also means that, for example, it is not possible to set up semiconductor's electronic properties as well tailored towards the intricacies of thin film solar cells, as SCAPS can. One other example is that CIGS, does not exist in an undoped state, meaning that the ability of *CHARGE* to automatically calculate the effects of a certain doping concentration on the characteristics of the intrinsic material, and, thus, the effects on the simulated device, acts as a constraint in the case of CIGS solar cells. The simulations cannot accurately be run without the doping concentration simulation object present, thus a work-around needs to be put in place, in order to more accurately simulate the self-doping CIGS absorber. To overcome this obstacle, the CIGS semiconductor model must initially be defined in an "undoped" state, with its parameters taking into account that a certain dopant level will be added afterwards, bringing the semiconductor properties into the desired level. Most existing CIGS models found in the literature for SCAPS, can be used, but require certain parameters adjustments, as for example, *CHARGE* requires the work function of a material, instead of the electron affinity required by SCAPS.

4.1 SCAPS electrical simulations

The model simulated by SCAPS aims to describe the best performance of the 2000 nm CIGS solar cell proposed architecture, through the validation of the figures of merit values comparing with the ones experimentally reported for the champion cell (22.6 %) with equivalent architecture [70]. To develop a robust SCAPS model to describe the current CIGS technology, several parameters have been updated, namely optical properties that were obtained through 3D FDTD optical simulations. An important accuracy boost in the model was the update of the rear and front optical reflection values through FDTD simulation reflection data. It is important to note that in SCAPS simulations, a bandgap grading profile in CIGS was defined according to the experimental champion solar cell. However, in the FDTD simulations it was only considered the minimum bandgap value. In order to replicate the champion device bandgap profile in the *Lumerical* FDTD software, several finite CIGS layers with different optical properties need to be used. The presence of several CIGS layers with different refractive index values produced additional interference fringes in the optical reflection data at the NIR wavelength range. Therefore, the replication of the bandgap profile was discarded due to unrealistic interference fringes at the optical front reflection together with an increased simulation complexity. For this Section, the CIGS optical constants were taken from [73], where a complete database of the optical properties of CIGS absorber layers with different GGI values is presented, allowing to simulate the gradient profile existent in the champion solar cell architecture.

The reflection of the Mo substrate was simulated with the FDTD simulation region inside a medium with n of 3. This value corresponds to the mean value of the CIGS material. The fixed refractive index is an approximation of the reality due to the variation of this index with wavelength (index variation of 2.8 to 3.2). The rear optical reflection obtained through the 3D FDTD optical simulations and used in the SCAPS-1D model is presented in Figure 12 a), together with the impact in the external quantum efficiency (EQE) curve, which may be seen by comparing both EQE curves of equivalent solar cells with implemented rear optical reflection from *Lumerical* and set at 0 %. With *Lumerical's* rear optical reflection, there is an improvement in the light absorption for the IR region, describing in a more suitable way the behavior of a real device. Hence, a certain percentage of light in this region of the spectrum reaches the Mo rear contact and is reflected back to the absorber, enabling a second pass in the CIGS layer, increasing its probability to be absorbed.

The front optical reflection defined in the SCAPS model is also provided by 3D FDTD optical simulations. To obtain an experimentally based model that can be compared with high-efficiency CIGS solar cells, an AR layer at the front contact was considered. Furthermore, the thickness of such layer was optimized to achieve the highest J_{sc} value. Additionally, atomic force microscopy experimental measurements provided the CIGS roughness from a complete solar cell, which was implemented in the FDTD optical simulations. The front optical reflection with the optimized AR layer with a thickness of 113 nm coupled with CIGS roughness is presented in Figure 12 b). It is important to refer the 1 nm difference between the thickness attained with this optimization and the optimized AR layer thickness in Section 3. This difference stems from slightly different thicknesses of the TCO layers and optical properties of the CIGS absorber, as the SCAPS model was validated through the employment of a highly efficient thin film architecture [70]. Figure 12 b) also presents the EQE response curve obtained with the SCAPS model with fully optimized rear and front reflections, and the EQE curve obtained from just the optimization of the rear reflection. For comparison purposes, the EQE of the 22.6 % efficient solar cell champion device is included in the Figure. The SCAPS model with rear and front optical reflections from FDTD simulations produces an overall good fit with the experimental high-efficiency device regarding the EQE response curves. However, the interference fringes are different between both curves, which is explained by the different CIGS roughness that is rather variable and process-dependent. Finally, in Figure 12 c) the comparison between the current density vs voltage (J-V) characteristic curves obtained by the SCAPS electrical model and the champion cell is shown. The SCAPS model was able to describe the behavior of an experimental high-efficiency CIGS solar cell device by incorporating the FDTD simulation results. The observation of the results in Figure 12 c) shows the accuracy of the SCAPS model describing the experimental high-efficiency device. Hence, the open circuit voltage (V_{oc}) and fill factor (FF) values are well modelled, mainly due to experimentally updated parameters and some included post deposition treatments effects, which will be reported in future contributions. Moreover, the optical reflection data from FDTD simulations was essential to provide a solid model regarding the optical performance and depicted by the similar J_{sc} values between both J-V characteristic curves. Therefore, bringing together the electrical and optical simulation tools, FDTD and SCAPS respectively, allows for the creation of a robust model that can effectively describe experimental champion solar cells.
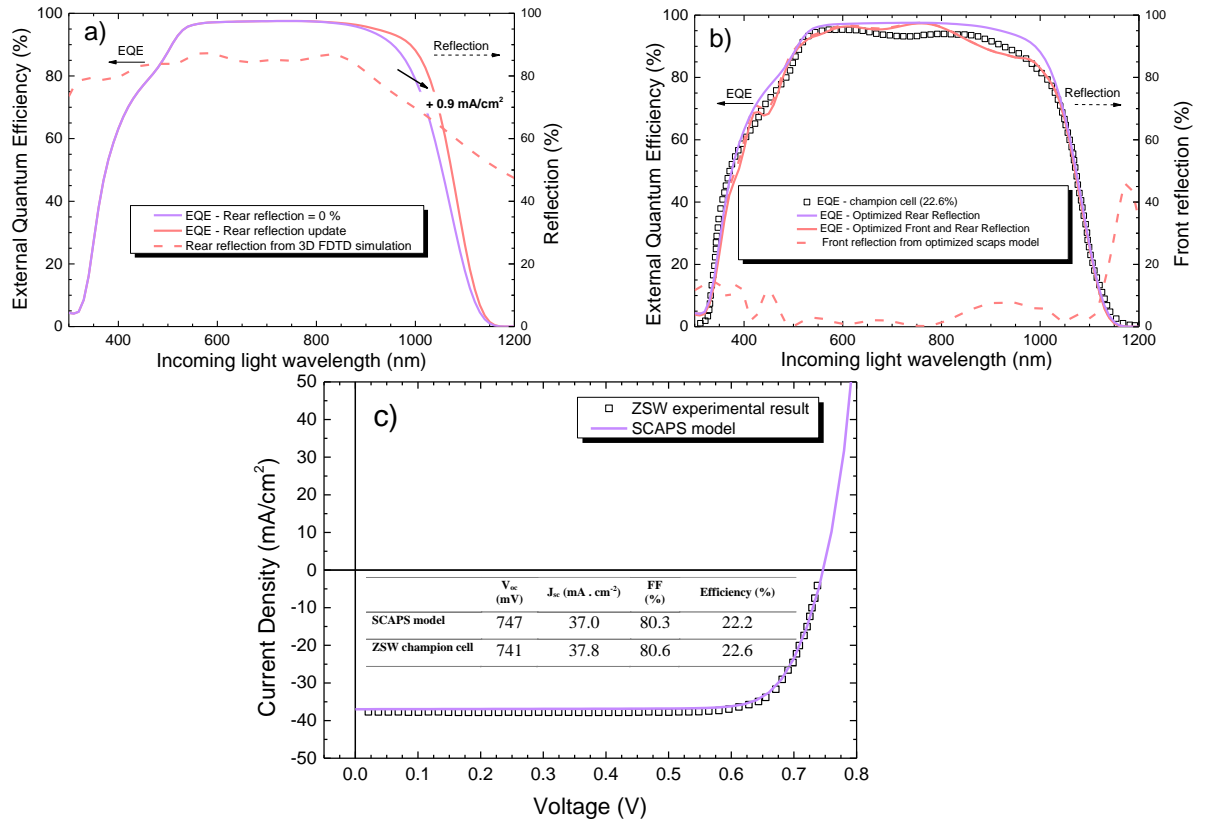
Figure 12. a) EQE response curves comparing the rear optical reflection of 0 % with the presented Mo rear optical reflection (dashed line) obtained with the 3D FDTD optical simulations in a 2000 nm thin film CIGS solar cell. Note that the front optical reflection is defined to 0 %; b) EQE response curve considering: the optimized rear reflection with front reflection equal to 0 %, the optimized AR layer and additional CIGS roughness used in the SCAPS model at the front contact and the experimental record cell; c) J-V curve comparison between the SCAPS model and the experimental result of the champion cell.

4.2 3D electrical Simulations Charge

Lumerical FDTD studies rely on the determination of the optical absorption of each layer, calculated through the FDTD method, and its dependence on the properties of the incident spectrum. Through the optical absorption rate, it is possible to calculate the number of generated charge carriers, the 2D and/or 3D distribution of said G per each of the incident wavelengths. To know how the performance of the solar cell will be affected, when the charge transport mechanics are considered, the architecture needs to be studied under a charge transport simulator [74]. However, a purely electronic study cannot accurately describe a CIGS solar cell on its own. As previously shown by the FDTD analysis, the charge carrier generation is not homogenous in the CIGS absorber, and it will vary depending on the optical architecture in place. Thus, the charge carrier generation distribution needs to be transported from the FDTD analysis, into the *Lumerical CHARGE*, such that the electronic analysis can take into consideration the optical properties in the density of charge carrier generation. However, prior to the electrical study with *Lumerical CHARGE*, the charge carrier generation distribution can provide information beyond the total solar cell J_{SC} value. By integrating the charge carrier distribution through the length and width of the CIGS absorber, multiplying it by q and plotting the resulting J_{SC} value in relation to the thickness of the absorber, the relationship between the generated current and the thickness depth at the absorber can be seen. As an example, a study was performed about a metallic rear reflector, deposited on the Mo rear contact. In CIGS solar cells, patterned dielectric layers can be used to encapsulate a highly reflective metal, allowing for both an interfacial passivation effect, as well as an enhanced optical reflection effect, as explained in Section 3 [14,48]. Since the 25 nm rear reflector's metal (Al) had to be shielded from the CIGS layer, in order to avoid unwanted metallic diffusion into the absorber, it was encapsulated with a 20 nm SiO$_x$ film, with the dielectric not only acting as a diffusion barrier, but as a passivation layer as well [7]. The previously described current generation thickness dependence was calculated for the referred architecture, and the results are shown in Figure 13 a), as well as an illustration of the design in question. In this example, there are two noticeably different

curves, with the encapsulated sample showing higher total current, in comparison to a reference ultrathin CIGS solar cell. Furthermore, the current augments are located close to the Mo rear contact, with the current increase due to the optically enhanced rear reflector and dielectric layer. With this data, the importance of the passivation layer is brought to the forefront. It shows that the optical gains are located close to the highly recombinative rear interface, meaning that if the current gains are to be taken advantage off to their fullest potential, the rear contact interface has to be passivated, and thus, the recombination velocity reduced [74]. The *Lumerical CHARGE* simulations can provide more detail about the solar cell architectures. For instance, the extraction method of the EQE of a solar cell device can be mimicked and extrapolated into the *Lumerical CHARGE* simulations, enabling to attain the EQE plot and charge extraction ratios. The charge carrier generation distribution can be exported with either the wavelength information integrated into a single distribution, or it can be exported with it containing the information for every single simulated wavelength value. To calculate the EQE through *Lumerical CHARGE* simulations, the latter needs to be performed, and the electrical simulations need to be carried out for every single wavelength value at short circuit conditions. Afterwards, the current attained through the electrical simulations is compared with the current values calculated through the FDTD simulations, and the ratio of how successfully the charge carriers are extracted is calculated. For instance, if through FDTD a current of 0.5 mA/cm^2 is calculated for a given wavelength value, but through CHARGE the resulting current for the same wavelength is 0.3 mA/cm^2, the ratio of the successfully extracted charge carrier is 0.6. By repeating this process for the entire spectrum, the complete charge extraction ratio profile can be calculated. Afterwards, the resulting optical absorption calculated through FDTD can be multiplied by said extraction ratio, and the resulting data is the solar cell's EQE. An example of the results achieved by the process described can be seen in Figure 13 b), where an ultrathin reference and a solar cell with back reflector and a dielectric encapsulation are compared. Through the resulting EQE's and charge extraction ratios, the effectiveness of the passivation layer and optical reflector is demonstrated. The former in the higher extraction ratio of the passivated solar cell, while the latter shows itself in the higher resulting photocurrent of the encapsulated solar cell once again.
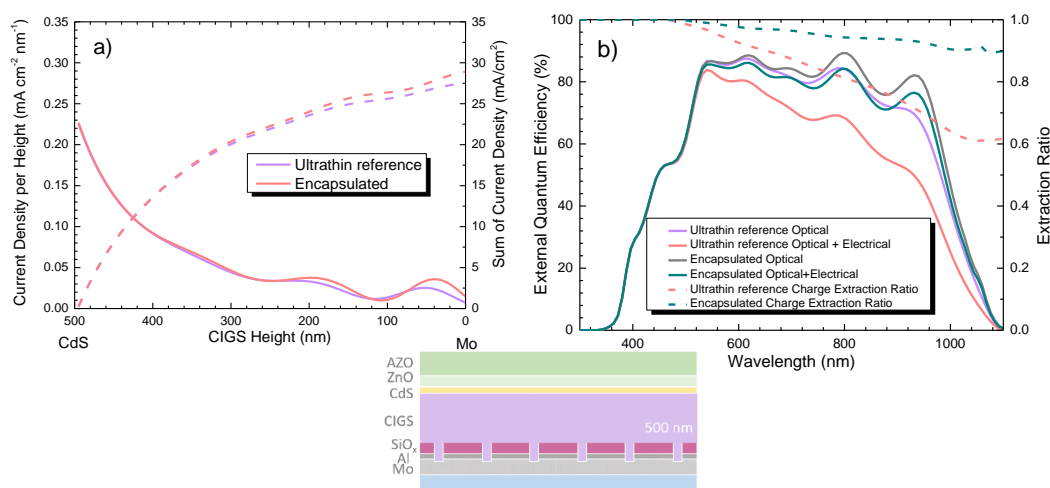

Figure 13. a) Current density generated throughout the thickness of the CIGS layer (dashed lines represent the current density sum); b) Simulated EQE with and without charge transport mechanics of passivated and reference solar cells. The charge carrier extraction ratio per wavelength is shown with the respective axis on the right side. Schematic representation of the CIGS solar cells stack architecture with an encapsulated Al layer.

5. CONCLUSIONS

A showcase of the potential of combining optical and electrical models to efficiently characterize a solar cell stack with the complex quaternary compound, that is CIGS, is demonstrated. The FDTD *Lumerical* software enables the realization of accurate simulations over a great variety of complex and exotic geometries that can provide a detailed insight over light management architectures in ultrathin CIGS solar cells. A detailed review of several light management approaches capable of improving the optical performance of ultrathin CIGS solar cell devices, through FDTD optical simulations is also presented, demonstrating the capability of this approach to accurately simulate and describe the optical benefits of exotic photonic or plasmonic light management architectures. The realistic light management architectures were simulated in a

ultrathin solar cell device capable of surpassing the optical performance of a typical thin film (2000 nm) CIGS solar cell, translated in a 6.15 mA/cm^2 enhancement of the short-circuit current over an ultrathin reference device, and 2.26 mA/cm^2 over the thin one. Furthermore, the FDTD software can also support and complement electrical simulations performed through the 1D SCAPS and 3D CHARGE software. The 1D SCAPS simulations supported through optical data extracted from FDTD optical simulations were validated by the comparison with the champion solar cell holding the record efficiency for the studied architecture. The potential of the FDTD and 3D CHARGE simulations was also demonstrated, where a novel approach of simulating the EQE of a solar cell device with a complex rear architecture is demonstrated. This study shows, through optical and electrical simulations, the potential of the CIGS ultrathin technology to meet the global electrical demand, as a "green" and sustainable competitor to the current PV market players.

ACKNOWLEDMENTS

REFERENCES

[1] Nakamura, M., Yamaguchi, K., Kimoto, Y., Yasaki, Y., Kato, T. and Sugimoto, H., "Cd-Free Cu (In,Ga)(Se,S)$_2$ Thin-Film Solar Cell With Record Efficiency of 23.35 %," IEEE J. of Photovoltaics, **9** (6), 1863–1867 (2019).

[2] Wilson, G.M., Al-Jassim, M., Metzger, W.K., Glunz, S.W., Verlinden, P., Xiong, G., Mansfield, L.M., Stanbery, B.J., Zhu, K., Yan, Y., Berry, J.J., Ptak, A.J., Dimroth, F., Kayes, B.M., Tamboli, A.C., Peibst, R., Catchpole, K., Reese, M.O., Klinga, C.S., Denholm, P., Morjaria, M., Deceglie, M.G., Freeman, J.M., Mikofski, M.A., Jordan, D.C., Tamizhmani, G., and Sulas-Kern, D.B., "The 2020 photovoltaic technologies roadmap. J. Phys. D. Appl. Phys., 53 (49), 493001 (2020).

[3] Teixeira, J.P., Salomé, P.M.P., Alves, B., Edoff, M., and Leitão, J.P., "Evidence of Limiting Effects of Fluctuating Potentials on V$_{oc}$ of Cu (In,Ga)Se$_2$ Thin-Film Solar Cells," Phys. Rev. Appl., 11 (5), 054013 (2019).

[4] Lindahl, J., Zimmermann, U., Szaniawski, P., Torndahl, T., Hultqvist, A., Salomé, P., Platzer-Björkman, C., and Edoff, M., "Inline Cu(In,Ga)Se2 co-evaporation for high-efficiency solar cells and modules," IEEE J. Photovoltaics, 3 (3), 1100–1105 (2013).

[5] Salomé, P.M.P., Rodriguez-alvarez, H., and Sadewasser, S., " Incorporation of alkali metals in chalcogenide solar cells," Sol. Energy Mater. Sol. Cells, 143, 9–20 (2015).

[6] Schleussner, S.M., Törndahl, T., Linnarsson, M., Zimmermann, U., Wätjen, T., and Edoff, M., "Development of gallium gradients in three-stage Cu (In,Ga)Se2 co-evaporation processes," Progress in Photovoltaics, 20 (3), 284–293 (2012).

[7] Cunha, J.M.V., Oliveira, K., Lontchi, J., Lopes, T.S., Curado, M.A., Barbosa, J.R.S., Vinhais, C., Chen, W.-C., Borme, J., Fonseca, H., Gaspar, J., Flandre, D., Edoff, M., Silva, A.G., Teixeira, J.P., Fernandes, P.A., and Salomé, P.M.P., " High-Performance and Industrially Viable Nanostructured SiO$_x$ Layers for Interface Passivation in Thin Film Solar Cells", Sol. RRL, 2000534 (2021).

[8] Gloeckler, M., Fahrenbruch, A.L., and Sites, J.R. " Numerical modeling of CIGS and CdTe solar cells: setting the baseline", Proc. 3rd World Conference on Photovoltaic Energy Conversion, 491–494 (2003).

[9] Hasheminassab, S.M.S., and Imanieh, M., "Influence of the Shape and Size of Ag Nanoparticles on the Performance Enhancement of CIGS Solar Cells: the Role of Surface Plasmons," Plasmonics, 16, 273–282 (2021).

[10] Kovačič, M., Krč, J., Lipovšek, B., Chen, W., Edoff, M., Bolt, P.J., Deelen, J. Van, Zhukova, M., Lontchi, J., Flandre, D., Salomé, P., and Topic, M. "Modelling Supported Design of Light Management Structures in Ultra-thin CIGS Photovoltaic Devices," Journal of Microelectronics, 49 (3), 183–190 (2019).

[11] Lontchi, J., Zhukova, M., Kovacic, M., Krc, J., Chen, W., Edoff, M., Bose, S., Salomé, P.M.P., Goffard, J., Cattoni, A., Gouillart, L., Collin, S., Gusak, V., and Flandre, D. "Optimization of Back Contact Grid Size in Al$_2$O$_3$-Rear-Passivated Ultrathin CIGS PV Cells by 2-D Simulations", IEEE J. of Photovoltaics, 10 (6), 1908–1917 (2020).

[12] Wang, Y., Chen, C., Su, T., Yang, T., Liu, W., Cheng, F., Wang, Z.M., and Chueh, Y. "Design of suppressing optical and recombination losses in ultrathin CuInGaSe$_2$ solar cells by Voronoi nanocavity arrays,". Nano

Energy, 78, 105225 (2020).

[13] Salomé, P.M.P., Vermang, B., Ribeiro-Andrade, R., Teixeira, J.P., Cunha, J.M.V., Mendes, M.J., Haque, S., Borme, J., Águas, H., Fortunato, E., Martins, R., González, J.C., Leitão, J.P., Fernandes, P.A., Edoff, M., and Sadewasser, S. "Passivation of Interfaces in Thin Film Solar Cells: Understanding the Effects of a Nanostructured Rear Point Contact Layer," Adv. Mater. Interfaces, *5* (2), 1–10 (2018).

[14] Lopes, T.S., Cunha, J.M.V., Bose, S., Barbosa, J.R.S., Borme, J., Donzel-Gargand, O., Rocha, C., Silva, R., Hultqvist, A., Chen, W.C., Silva, A.G., Edoff, M., Fernandes, P.A., and Salome, P.M.P. "Rear Optical Reflection and Passivation Using a Nanopatterned Metal/Dielectric Structure in Thin-Film Solar Cells". IEEE J. Photovoltaics, 9 (5), 1421-1427 (2019).

[15] Rahman, T., Fobelets, K., and Fobelets, K. "Efficient tool flow for 3D Photovoltaic modelling", Computer Physics Communications, 193, 124-130 (2015).

[16] Sayeed, A., and Rouf, H.K. "Numerical Simulation of Thin Film Solar Cell Using SCAPS-1D : ZnSe as Window Layer". Proc. of 2019 22nd Int. Conf. Comput. Inf. Technol., (1–5 (2019).

[17] Pettersson, J., Zimmermann, U., and Edoff, M. "Baseline model of graded-absorber $Cu(In,Ga)Se_2$ solar cells applied to cells with $Zn_{1-x}Mg_xO$ buffer layers," Thin Solid Films, 519 (21), 7476–7480 (2011).

[18] Burgelman, M., Nollet, P., and Degrave, S., "Modelling polycrystalline semiconductor solar cells,", Thin Solid Films, 361-362, 527–532 (2000).

[19] Ansys/Lumerical, [Lumerical FDTD Solutions Reference Manual] (2014).

[20] "Finite Difference Time Domain (FDTD) solver introduction", https://support.lumerical.com/hc/en-us/articles/360034914633-Finite-Difference-Time-Domain-FDTD-solver-introduction (06 February 2021).

[21] Carron, R., Avancini, E., Feurer, T., Bissig, B., Losio, P.A., Figi, R., Schreiner, C., Bürki, M., Bourgeois, E., Remes, Z., Nesladek, M., Buecheler, S., and Tiwari, A.N. "Refractive indices of layers and optical simulations of $Cu(In,Ga)Se_2$ solar cells". Sci. Technol. Adv. Mater., 19 (1), 396–410 (2018).

[22] Beal, A. R. and Hughes, H. P. "Kramers-Kronig analysis of the reflectivity spectra of $2H-MoS_2$, $2H-MoSe_2$ and $2H-MoTe_2$,"J. Phys. C Solid State Phys., 12, 881–890 (1979).

[23] Werner, W.S.M., Glantschnig, K., and Ambrosch-Draxl, C. "Optical constants and inelastic electron-scattering data for 17 elemental metals," J. Phys. Chem. Ref. Data, 38 (4), 1013–1092 (2009).

[24] Mendes, M.J., Haque, S., Sanchez-Sobrado, O., Araújo, A., Águas, H., Fortunato, E., and Martins, R. "Optimal-Enhanced Solar Cell Ultra-thinning with Broadband Nanophotonic Light Capture," iScience, 3, 238–254 (2018).

[25] Schmid, M. "Review on light management by nanostructures in chalcopyrite solar cells," Semicond. Sci. Technol., 32 (4), 043003 (2017).

[26] Oliva, A. I., Solís-Canto, O., Castro-Rodríguez, R. and Quintana, P. "Formation of the band gap energy on CdS thin films growth by two different techniques," Thin Solid Films, 391 (1), 28–35 (2001).

[27] Kapilashrami, M., Kronawitter, C.X., Törndahl, T., Lindahl, J., Hultqvist, A., Wang, W.C., Chang, C.L., Mao, S.S., and Guo, J. "Soft X-ray characterization of $Zn_{1-x}Sn_xO_y$ electronic structure for thin film photovoltaics," Phys. Chem. Chem. Phys., 14 (29), 10154–10159 (2012).

[28] Witte, W., Spiering, S., and Hariskos, D. "Substitution of the CdS buffer layer in CIGS thin-film solar cells: Status of current research and record cell efficiencies," Vak. Forsch. und Prax., 26 (1), 23–27 (2014).

[29] Shockley, W. and Queisser, H. J. "Detailed balance limit of efficiency of p-n junction solar cells," J. Appl. Phys., 32, 510–519 (1961).

[30] Sun, C., and Wang, X. "Efficient Light Trapping Structures of Thin Film Silicon Solar Cells Based on Silver Nanoparticle Arrays," Plasmonics, 10 (6), 1307–1314 (2015).

[31] Lee, S., Park, J., Yi, J., and Jeong, C. "Improvement of a-Si:H Thin-film Solar Cells by Employing Large Ag Nanoparticles" Isr. J. Chem., 55(10), 1103–1108 (2015).

[32] Liu, D., and Wang, Q., "Light-trapping surface coating with concave arrays for efficiency enhancement in amorphous silicon thin-film solar cells," Opt. Commun., 420, 84–89 (2018).

[33] Yu, Z., Raman, A., and Fan, S. "Fundamental limit of nanophotonic light trapping in solar cells," Proc. Natl. Acad. Sci. U. S. A., 107 (41), 17491–17496 (2010).

[34] Deka, N., and Changmai, P. "A Review on Light Trapping Capacities of Different Photovoltaic Cells" ABDU Journal of Electrical and Electronical Engineering, 1 (2), 18–28 (2017).

[35] Kang, G., Yoo, J., Ahn, J., and Kim, K. "Transparent dielectric nanostructures for efficient light management in optoelectronic applications," Nano Today, 10 (1), 22–47 (2015).

[36] Hu, Y.-H., Chen, Y.-C., Xu, H.-J., Gao, H., Jiang, W.-H., Hu, F., and Wang, Y.-X. "Texture ZnO Thin-Films and their Application as Front Electrode in Solar Cells," Engineering, 02 (12), 973–978 (2010).

[37] Owen, J.I., Hüpkes, J., Zhu, H., Bunte, E., and Pust, S.E. "Novel etch process to tune crater size on magnetron sputtered ZnO:Al," Phys. Status Solidi Appl. Mater. Sci., 208 (1), 109–113 (2011).

[38] Seo, B.H., Lee, S.H., Seo, J.H., Jeon, J.H., and Choe, H.H. "Study on the wet etch behavior of a zinc-oxide semiconductor in acid solutions," J. Korean Phys. Soc., 53 (1), 402–405 (2008).

[39] Hüpkes, J., Owen, J.I., Pust, S.E., and Bunteâ "Chemical etching of zinc oxide for thin-film silicon solar cells," ChemPhysChem, 13 (1), 66–73 (2012).

[40] Payne, D.N.R., Boden, S.A., Clark, O.D., Delahoy, A.E., and Bagnall, D.M. "Characterization of experimental textured ZnO:Al films for thin film solar cell applications and comparison with commercial and plasmonic alternativesc," Proc. of Conf. Rec. IEEE Photovolt. Spec. Conf., 1560–1564 (2010).

[41] Yan, X., Venkataraj, S., and Aberle, A.G., "Wet-chemical surface texturing of sputter-deposited ZnO:Al films as front electrode for thin-film silicon solar cells." Int. J. Photoenergy, 2015, 548984 (2015).

[42] Müller, J., Schöpe, G., Kluth, O., Rech, B., Ruske, M., Trube, J., Szyszka, B., Höing, T., Jiang, X., and Brauer, G. "Texture-etched zinc oxide substrates for silicon thin film solar cells-from laboratory size to large areas," Proc of Conf. Rec. IEEE Photovolt. Spec. Conf., 758–761 (2000).

[43] Cho, C., Kim, H., Jeong, S., Baek, S.W., Seo, J.W., Han, D., Kim, K., Park, Y., Yoo, S., and Lee, J.Y. "Random and V-groove texturing for efficient light trapping in organic photovoltaic cell,". Sol. Energy Mater. Sol. Cells, 115, 36–41 (2013).

[44] Amalathas, A.P., and Alkaisi, M.M. "Nanostructures for light trapping in thin film solar cells," Micromachines, 10 (9), 619 (2019).

[45] Čampa, A., Krč, J., Malmström, J., Edoff, M., Smole, F., and Topič, M. "The potential of textured front ZnO and flat TCO/metal back contact to improve optical absorption in thin Cu(In,Ga)Se$_2$ solar cells," Thin Solid Films, 515, 5968–5972 (2007).

[46] Dahan, N., Jehl, Z., Hildebrandt, T., Greffet, J.J., Guillemoles, J.F., Lincot, D., and Naghavi, N. "Optical approaches to improve the photocurrent generation in Cu(In,Ga)Se$_2$ solar cells with absorber thicknesses down to 0.5 μm," J. Appl. Phys., 112 (9), 094902 (2012).

[47] Bharat Bhushan, [Encyclopedia of Nanotechnology], Springer, Netherlands (2007).

[48] Oliveira, A.J.N., de Wild, J., Oliveira, K., Valença, B.A., Teixeira, J.P., Guerreiro, J.R.L., Abalde-Cela, S., Lopes, T.S., Ribeiro, R.M., Cunha, J.M.V., Curado, M.A., Monteiro, M., Violas, A., Silva, A.G., Prado, M., Fernandes, P.A., Vermang, B., and Salomé, P.M.P. "Encapsulation of Nanostructures in a Dielectric Matrix Providing Optical Enhancement in Ultrathin Solar Cells," Sol. RRL, 4 (11), 2000310..

[49] Ong, K.H., Agileswari, R., Maniscalco, B., Arnou, P., Kumar, C.C., Bowers, J.W., and Marsadek, M.B. "Review on Substrate and Molybdenum Back Contact in CIGS Thin Film Solar Cell," International Journal of Photoenergy, 2018, 9106269 (2018).

[50] Feurer, T., Reinhard, P., Avancini, E., Bissig, B., Löckinger, J., Fuchs, P., Carron, R., Weiss, T.P., Perrenoud, J., Stutterheim, S., Buecheler, S., and Tiwari, A.N. "Progress in thin film CIGS photovoltaics – Research and development, manufacturing, and applications," Prog. Photovoltaics Res. Appl., 25 (7), 645–667 (2018).

[51] Scheer, R., and Schock, H.-W., [Chalcogenide Photovoltaics Physics, Technologies, and Thin Film Devices] Wiley-VCH, Berlin, 2011.

[52] P. M. P. Salomé, "Chalcogenide Thin Films for Solar Cells: Growth and Properties", Doctoral Dissertation, Universidade de Aveiro, 2011.

[53] Mendes, M.J., Morawiec, S., and Simone, F. "Colloidal plasmonic back reflectors for light trapping in solar cells," Nanoscale, 2014, 6, 4796-4805 (2014).

[54] Bose, S., Cunha, J.M. V., Suresh, S., De Wild, J., Lopes, T.S., Barbosa, J.R.S., Silva, R., Borme, J., Fernandes, P.A., Vermang, B., and Salomé, P.M.P. "Optical Lithography Patterning of SiO$_2$ Layers for Interface Passivation of Thin Film Solar Cells," Sol. RRL, 2 (12), 1800212 (2018).

[55] Huang, Y., Sahraei, N., Widenborg, P.I., Marius, I., Kumar, G., Iskander, A., and Aberle, A.G. "Enhanced light trapping in polycrystalline silicon thin-film solar cells using plasma-etched submicron textures," Sol. Energy Mater. Sol. Cells, **122**, 146–151 (2014).

[56] Morawiec, S., Mendes, M.J., Filonovich, S.A., Mateus, T., Mirabella, S., Águas, H., Ferreira, I., Simone, F., Fortunato, E., Martins, R., Priolo, F., and Crupi, I. "Broadband photocurrent enhancement in a-Si:H solar cells

with plasmonic back reflectors," Opt. Express, 22 (S4), A1059 (2014).

[57] Garcia, M.A. "Surface plasmons in metallic nanoparticles : fundamentals," Journal of Physics D: Applied Physics, Volume 44 (28), 283001 (2011).

[58] Shafiqaa, A.R., Azizb, A.A., and Mehrdel, B. "Nanoparticle Optical Properties : Size Dependence of a Single Gold Spherical," J. Phys. Conf. Ser., 1083, 012040 (2018).

[59] Morawiec, S., Mendes, M.J., Filonovich, S.A., Mateus, T., Mirabella, S., Águas, H., Ferreira, I., Simone, F., Fortunato, E., Martins, R., Priolo, F., and Crupi, I. " Broadband photocurrent enhancement in a-Si:H solar cells with plasmonic back reflectors," Opt. Express, 22 (S4), A1059 (2014).

[60] Harrison, R. "Mechanisms and applications of near-field and far-field enhancement using plasmonic nanoparticles", Doctoral Dissetation, University of Texas, 2012.

[61] Akimov, Y.A., Koh, W.S., Sian, S.Y., Ren, S., Akimov, Y.A., Koh, W.S., Sian, S.Y., and Ren, S. "Nanoparticle-enhanced thin film solar cells : Metallic or dielectric nanoparticles?" Appl. Phys. Lett. 96 (7), 073111 (2010).

[62] Bose, S., Cunha, J.M.V., Borme, J., Chen, W.C., Nilsson, N.S., Teixeira, J.P., Gaspar, J., Leitão, J.P., Edoff, M., Fernandes, P.A., and Salomé, P.M.P. "A morphological and electronic study of ultrathin rear passivated Cu(In,Ga)Se$_2$ solar cells," Thin Solid Films, 671 (1), 77–84 (2017).

[63] Ledinek, D., Salomé, P., Hägglund, C., Zimmermann, U., and Edoff, M. "Rear Contact Passivation for High Bandgap Cu(In, Ga)Se$_2$ Solar Cells with a Flat Ga profile," IEEE J. Photovoltaics, 8 (3), 864–870 (2018).

[64] Curado, M.A., Teixeira, J.P., Monteiro, M., Ribeiro, E.F.M., Vilão, R.C., Alberto, H. V., Cunha, J.M.V., Lopes, T.S., Oliveira, K., Donzel-Gargand, O., Hultqvist, A., Calderon, S., Barreiros, M.A., Chiappim, W., Leitão, J.P., Silva, A.G., Prokscha, T., Vinhais, C., Fernandes, P.A., and Salomé, P.M.P. "Front passivation of Cu(In,Ga)Se$_2$ solar cells using Al$_2$O$_3$: Culprits and benefits," Appl. Mater. Today, 21, 100867 (2020).

[65] Cunha, J.M. V., Lopes, T.S., Bose, S., Hultqvist, A., Chen, W.-C., Donzel-Gargand, O., Ribeiro, R.M., Oliveira, A.J.N., Edoff, M., Fernandes, P.A., and Salome, P.M.P., "Decoupling of Optical and Electrical Properties of Rear Contact CIGS Solar Cells," IEEE J. Photovoltaics, 9 (6), 1857–1862 (2019)

[66] Cunha, J.M.V., Fernandes, P.A., Hultqvist, A., Teixeira, J.P., Bose, S., Vermang, B., Garud, S., Buldu, D., Gaspar, J., Edoff, M., Leitao, J.P., and Salome, P.M.P., "Insulator Materials for Interface Passivation of Cu(In,Ga)Se2 Thin Films," IEEE J. Photovoltaics, 8 (5), 1313–1319 (2018).

[67] Lare, C. Van, Yin, G., Polman, A., and Schmid, M. "Light Coupling and Trapping in Ultrathin Cu(In,Ga)Se2 Solar Cells Using Dielectric Scattering Patterns," ACS Nano, 9, 10, 9603–9613 (2015).

[68] Yin, G., Manley, P., and Schmid, M. "Light trapping in ultrathin CuIn$_{1-x}$Ga$_x$Se$_2$ solar cells by dielectric nanoparticles," 163 (15), 443–452 (2018).

[69] Hegedus, S.S., and Shafarman, W.N. "Thin-film solar cells: device measurements and analysis," Prog. Photovoltaics Res. Appl., 12 (23), 155–176 (2004).

[70] Jackson, P., Wuers, R., Hariskos, D., Lotter, E., Witte, W. and Powalla M., "Effects of heavy alkali elements in Cu(In,Ga)Se$_2$ solar cells with efficiencies up to 22.6%," Phys. Status Solidi - Rapid Res. Lett., 10 (8), 583–586 (2016).

[71] Decock, K., Khelifi, S., and Burgelman, M. "Modelling multivalent defects in thin film solar cells," Thin Solid Films, 519 (21), 7481–7484 (2011).

[72] Burgelman, M., Decock, K., Khelifi, S., and Abass, A. "Advanced electrical simulation of thin film solar cells," Thin Solid Films, 535 (1), 296–301 (2013).

[73] Minoura, S., Kodera, K., Maekawa, T., Miyazaki, K., Niki, S., and Fujiwara, H. "Dielectric function of Cu(In, Ga)Se$_2$-based polycrystalline materials," J. Appl. Phys., 113 (6), 063505 (2013).

[74] "CHARGE solver introduction – Lumerical Support", https://support.lumerical.com/hc/en-us/articles/360034917693-CHARGE-solver-introduction, (06 February 2021).